Journal of Power Sources 261 (2014) 378–388

Contents lists available at ScienceDirect

Journal of Power Sources

journal homepage: www.elsevier.com/locate/jpowsour

Battery cycle life balancing in a microgrid through flexible distribution of energy and storage resources

Hussam J. Khasawneh*, Mahesh S. Illindala

Electrical and Computer Engineering, The Ohio State University, 205 Dreese Labs, 2015 Neil Avenue, Columbus, OH 43210, USA

HIGHLIGHTS

- A microgrid consisting of small-rated fuel cell-battery hybrid DERs was modeled.
- Battery utilization was found to vary significantly due to its 'electrical' placement.
- Solutions for balancing battery lifetimes based on FDERS were introduced.
- Solutions were based on implementing 'virtual' reactances without physical changes.
- Results showed that battery lifetime can be balanced and extended by 76%.

ARTICLE INFO

Article history:
Received 5 September 2013
Received in revised form
31 January 2014
Accepted 7 February 2014
Available online 20 February 2014

Keywords:
Aging
Distributed control
Distributed generation
Fuel cell
Li-ion battery
Virtual reactance

ABSTRACT

In this paper, a microgrid consisting of four fuel cell-battery hybrid Distributed Energy Resources (DERs) is devised for an industrial crusher–conveyor load. Each fuel cell was accompanied by a Li-ion battery to provide energy storage support under islanded condition of the microgrid since the fuel cells typically have poor transient response characteristics. After carrying out extensive modeling and analysis in MATLAB®, the battery utilization was found to vary significantly based on the DER's 'electrical' placement within the microgrid. This paper presents, under such conditions, a variety of battery life balancing solutions through the use of the new framework of Flexible Distribution of EneRgy and Storage Resources (FDERS). It is based on an *in-situ* reconfiguration approach through 'virtual' reactances that help in changing the 'electrical' position of each DER without physically displacing any component in the system. Several possible approaches toward balancing the battery utilization are compared in this paper taking advantage of the flexibility that FDERS offers. It was observed that the estimated battery life is dependent on factors such as cycling sequence, pattern, and occurrence.

© 2014 Elsevier B.V. All rights reserved.

1. Introduction

Distributed Energy Resources (DERs) are being increasingly preferred to meet the growing needs of high energy consumers with minimal changes to the existing power grid. A microgrid is a smart electrical grid that consists of several DERs together with loads and energy storage devices, such as flywheels, super capacitors, and batteries [1]. The various kinds of primary energy sources employed include dispatchable as well as non-dispatchable resources like internal combustion engines, microturbines, photovoltaics, wind generators, and fuel cells [2]. Among them, even the dispatchable ones such as fuel cells have a long start-up time and poor transient response due to their inherent characteristics [3]. As such, they are supplemented with energy storage to meet the load demand under islanded-mode of operation, because the fuel cell falls short in supplying independently the transient load demand. Since batteries can offer rapid transient response with a higher specific power capacity compared to that of fuel cells, a combination of fuel cells with batteries is found to be advantageous for many applications [4,5]. The transient response of a typical fuel cell-battery hybrid DER is shown in Fig. 1, where P_L and P_{FC} denote the step change in load power demand and the fuel cell response, respectively [6]. The difference between the two responses P_L and P_{FC} causes charging and discharging cycles in the battery. It is well known that due to such repeated cycles, the deliverable capacity of a battery tends to decrease, and this *capacity fade* phenomenon is called *battery aging* [7,8]. Furthermore, a *power fade* comes into picture when the internal resistance of the cell increases [9]. *Cycle life* refers to the number of times a battery is cycled before the cell capacity *fades* below 80% of its nominal value according to the United States Advanced Battery Consortium (USABC) [10,11].

* Corresponding author. Tel./fax: +1 6144409024.
E-mail address: khasawneh.10@osu.edu (H.J. Khasawneh).

http://dx.doi.org/10.1016/j.jpowsour.2014.02.043
0378-7753/© 2014 Elsevier B.V. All rights reserved.

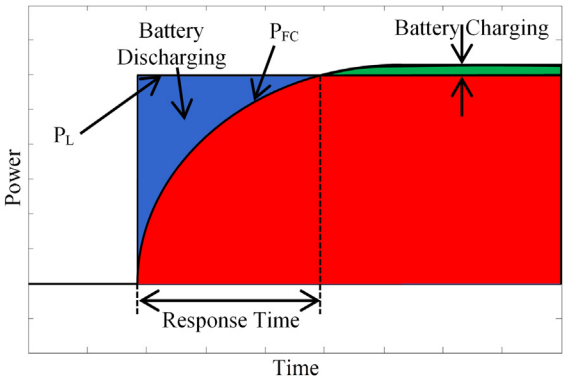

Fig. 1. Transient dynamic response of a fuel cell-battery hybrid system.

Batteries contain heavy metals including lithium, mercury, lead, cadmium, and nickel. Such metals can be harmful to the environment when batteries are improperly disposed [12]. Currently, there are regulations like the US Mercury-Containing and Rechargeable Battery Act of 1996 and the EU Directives 91/156 and 91/689 for battery waste management and sustainable development [13]. Therefore, extending the battery life has become a critical concern because they are the most expensive components in many hybrid applications. In this paper, a microgrid consisting of several small-rated fuel cell-battery hybrid DERs is considered for supplying a crusher–conveyor load when power from the main grid is not available, see Fig. 2. This paper shows that the battery cycle life can be extended in such a microgrid by creating a cooperative framework known as *Flexible Distribution of EneRgy and Storage Resources* (FDERS) that was recently introduced in Ref. [14].

FDERS was inspired by the V-shape formation of a flock of birds [15,16] and peloton/echelon formation of a cycling racing team [17–19], see Fig. 3. In this framework, the *pecking order* of DERs is determined on the basis of their relative strength at any time. It has been reported in Ref. [15] that the V-shape formation consisting of 25 birds can theoretically result in a 70% increase in the range of distance flown by them as compared with a bird flying alone. An occasional rotation of positions helps in reinvigorating all the members. In this paper, similar cooperative strategies are evaluated for balancing the battery cycle life in a parallel configuration of small-rated fuel cell-battery hybrid DERs supplying a large and fluctuating crusher–conveyor load, especially when there is no power available from the main (utility) grid.

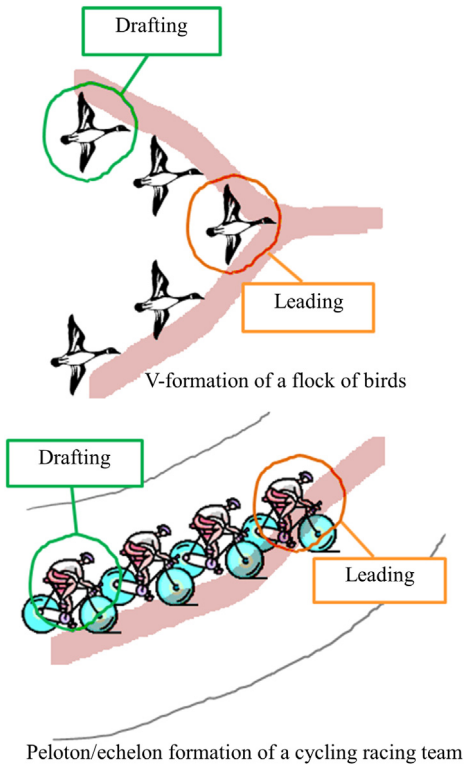

Fig. 3. Energy saving formations.

2. System description

The microgrid system of Fig. 2 considered in this paper is a practical scenario for supplying power to an industrial site comprising a large and fluctuating crusher–conveyor load.

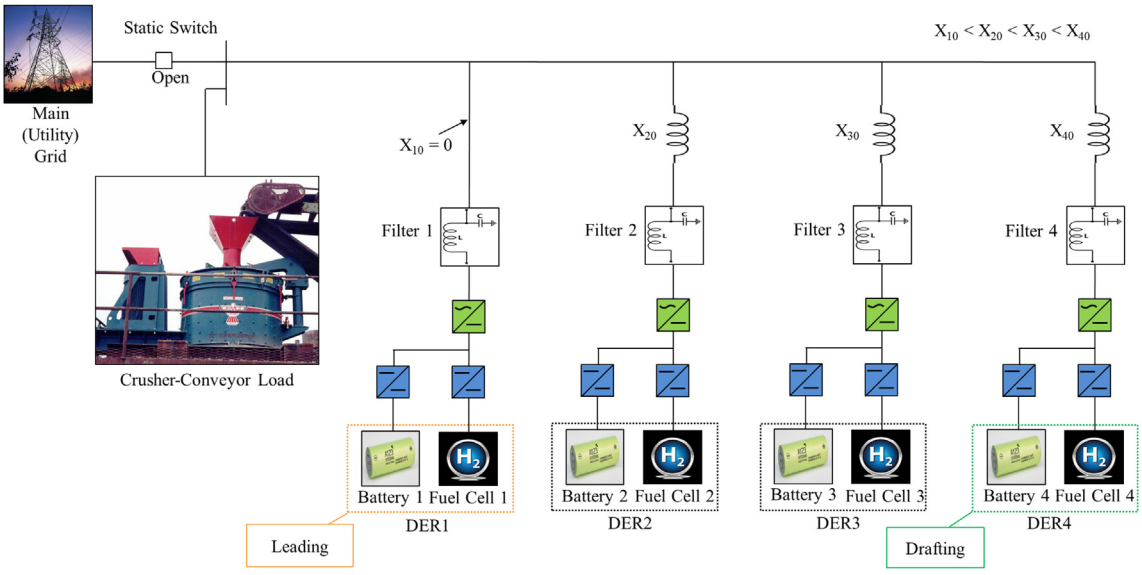

Fig. 2. Single-line diagram of a microgrid consisting of four fuel cell-battery hybrid DERs supplying a large and fluctuating crusher–conveyor load.

Table 1
Motor loading profiles for a 3-phase, 480-V crusher–conveyor (adapted from Ref. [20]).

Recurring cycles		
Time	RMS current (A)	Active power (P_L) (kW)
20 s	424	300
120 s	56	34
20 s	424	300
120 s	56	34
20 s	424	300
120 s	56	34
20 s	424	300
120 min	56	34

Numerous publications in the literature have reported the extremely demanding load profiles observed at industrial sites [20–22]. For the crusher–conveyor load profile tabulated in Table 1 [20] it is fair to assume that the recurring cycles repeat for five times in every 24 h of operation [23].

The microgrid consists of four fuel cell-battery hybrid DERs, each including a Solid Oxide Fuel Cell (SOFC) along with an A123 Li-ion battery pack ANR26650M1A [24]. These DERs are 'electrically' displaced by unequal reactances with the DER1 being the 'electrically' closest as depicted in Fig. 2 (*i.e.* $X_1 < X_2 < X_3 < X_4$). Such reactances are caused by the transformers, line filters, distribution lines, etc. For analyzing a more realistic system, DER units of unequal ratings were assumed. Each DER's battery is sized according to its rated power. The DERs design parameters are given in Table 2, and their interface reactances X_k included practical considerations of $X/R = 10\%$. Such microgrid models have been previously experimentally validated in laboratory [25] and on CERTS Microgrid field testbed [26]. The circuit details of DER components like power electronic DC/AC inverters, filters and transformers can be found in Refs. [27–29].

A block diagram depicting the power flows and controls in each fuel cell-hybrid DER is displayed in Fig. 4. As seen in this figure, a *power management system* regulates the fuel flow rate of fuel cell stack to meet the expected load demand [30]. Moreover, the power management system is aimed at splitting the power flow between the SOFC and Li-ion battery to sustainably meet its production demands [5]. In addition, it maximizes the fuel cell generation output to recharge the battery and cover parasitic losses of items such as pumps, fans, blowers and heat exchangers [31] (*cf.* Fig. 1). Also, the power management system maintains a fast recharge of the Li-ion battery at a constant rate of 5 C-rate. As a result, the battery would eventually become fully charged in steady state when the fuel cell fulfills the load demand. It is to be noted that the SOFC is connected to DC-link through a unidirectional DC/DC converter, unlike the Li-ion battery which is connected to a bi-directional DC/DC converter to allow charging and discharging.

In order to enable power sharing with decentralized controls of power electronics-based DERs in the microgrid [3], each DER unit is regulated by means of frequency/active power (ω/P) and voltage/reactive power (V/Q) droop controls, as shown in Fig. 5 [25,32]. The behavior of steady-state active power sharing between the interconnected DER units in a microgrid can be directly calculated from the steady-state frequency droop curves of the interconnected DER units. Normally, these droop characteristics are designed such that interconnected DERs under islanded conditions share the total power among themselves in a manner proportionate with their ratings. Moreover, each DER's steady-state power share is independent of its locational placement within the microgrid. It is to be noted that the reactive power control has no bearing on the battery lifetime/aging studies conducted in this paper, and hence its details have been omitted for brevity.

Table 2
DER ratings and design parameters.

DER_k	Rated power (kW)	X_k (Ω)	k_q (V kVAR^{-1})	k_p (rad kJ^{-1})	Battery module	
					In series (cells)	Nominal voltage (V)
1	30	0	0.01	0.0157	28	92.4
2	60	0.18	0.01	0.0079	56	184.8
3	90	0.27	0.01	0.0052	84	277.2
4	120	0.46	0.01	0.0039	112	369.6

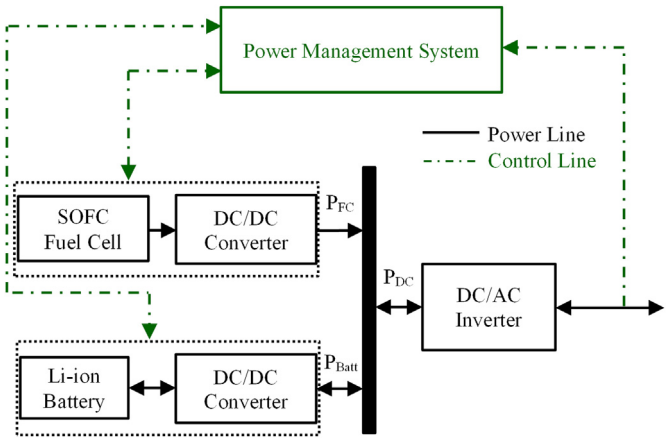

Fig. 4. Power flow and control structure of each fuel cell-battery hybrid DER.

3. System modeling and simulation strategy

A detailed and dynamic model for the four DER parallel connected microgrid has been developed in MATLAB®/Simulink™ with the power network simulated in SimPowerSystems™ toolbox as explained in Ref. [14]. The simulation is conducted in two stages, *viz.*, (i) time-domain simulation and (ii) offline calculations to estimate battery cycle life, as illustrated in Fig. 6. First, the time-domain simulation of green colored blocks is carried out iteratively for the entire time period. The generation output of each individual DER is computed when the system is subjected to the application load profile of crusher–conveyor load. This power is shared between the fuel cell and battery components. Later, the battery aging model, displayed in blue dashed lines in Fig. 6, is run offline for estimating the battery cycle life using the battery SoC and temperature data obtained from time-domain simulation over

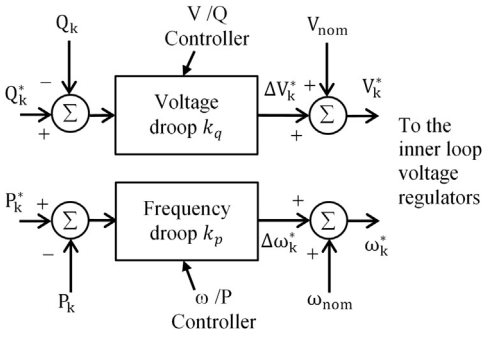

Fig. 5. DER outer loop power controller block diagram ($k = 1, 2, 3, 4$).

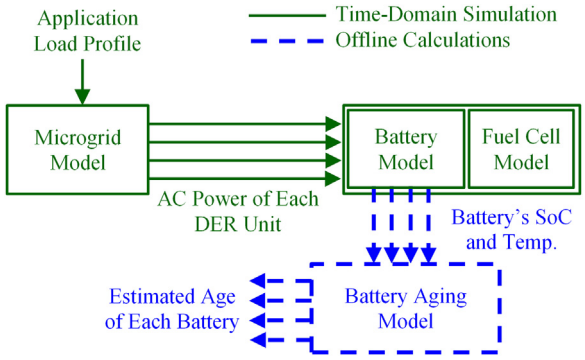

Fig. 6. Block diagram of simulation strategy for battery life estimation.

several cycles. A brief description of the utilized component models within each fuel cell-battery hybrid DER is described in this section.

3.1. Solid oxide fuel cell (SOFC) model

Fuel cells are considered to be one of the most promising alternative energy resources due to their high energy density, high efficiency, zero or low emission, and flexible modular structure [33]. Energy is produced in a fuel cell by oxidizing (O_2) the hydrogen gas (H_2). The resulting ions (OH^-) from the reaction at the anode fuse with the oxygen to become water (H_2O), and the resulting electrons form an electrical field between the anode and cathode through the external circuit [34]. Despite the unique advantage that fuel cells offer, they have slower response time to step changes in load demand due to their inherent characteristics.

This paper builds on a basic SOFC power dynamic model developed in Ref. [35] together with necessary enhancements for simulating the system's control strategies. Moreover, this model assumes that the fuel cell gases are ideal, the interior of the electrodes has the same pressure, and that the fuel cell temperature is invariant. Furthermore, since the chemical response in the fuel processor is usually slow, the dynamic response can be modeled as a first-order transfer function with a 10-s time constant. It is to be also noted that the model of SOFC power plant employed in this paper was adopted from that developed and validated earlier in Ref. [36].

3.2. Li-ion battery model

In this paper, the Li-ion battery is modeled on the basis of the Randle equivalent circuit phenomenological model [37]. This model consists of a voltage source (V_{oc}) and an internal resistance R_0 connected in series to n-times parallel RC circuits representing diffusion within a cell. All of them are dependent on the battery SoC and temperature.

The battery terminal voltage is computed as [38,39]:

$$V_{batt} = V_{oc} - R_0 I - \sum_{i=1}^{n} V_i \tag{1}$$

where V_{batt} is the battery terminal voltage, V_{oc} is the open circuit voltage, and V_i is the voltage across the ith parallel RC circuit. The number of RC circuits defines the order of the model. Of course, a higher order model provides an improved frequency response, leading to a better time-domain approximation, yet increasing the system's complexity. Therefore, a fairly reasonable order model has been employed. The simple structure and low computation effort of the low-order equivalent circuit models make them beneficial in designing control algorithms. It is to be noted that the control-oriented model for Li-ion battery was built on two platforms – thermal and electrical – as indicated in Fig. 7.

As seen in Fig. 7, the thermal model computes heat generated by the discharge current, and then determines the temperature of the battery, assuming that the battery temperature distribution is uniform in all directions at any instant of the transient heat transfer process. The battery temperature is determined by solving the differential equation [40]:

$$\frac{dT}{dt} = \frac{\dot{Q} - Ah(T - T_\infty)}{mc} \tag{2}$$

where $Ah(T - T_\infty)$ is the dissipated heat by convection, m is the mass, c is the specific thermal capacity, and $\dot{Q}$ is the heat generated by Joule effect in the battery which is given by:

$$\dot{Q} = RI^2 + \sum_{1}^{N} R_i I_i^2 \tag{3}$$

After computing the temperature, the battery model estimates the state of charge (SoC) by solving:

$$\mathrm{SoC}(t) = \mathrm{SoC}_0 - \int_0^t \frac{\eta I(t)}{C_n} dt \tag{4}$$

where SoC_0 is the initial state of charge, C_n is the nominal cell capacity, and η is the Coulombic efficiency factor that is assumed to be unity.

3.3. Battery aging model

Batteries are often classified into three categories – primary, secondary, or reserve [41]. While the primary batteries are made of chemical elements that cannot be electrically recharged, the secondary batteries can be discharged and then recharged repetitively. On the other extreme, the reserve batteries are designed for long-term storage. Therefore, this paper focuses on the secondary batteries, specifically the Li-ion batteries to meet the transient energy demands of the fast varying load demand in the proposed industrial plant.

In general, a battery has three main usage phases: charging, discharging, and resting. A discharge followed by a charge is called a *cycle*. The deliverable capacity of a Li-ion battery tends to decrease due to the cycling. This phenomenon is called *battery aging* [42–44]. Battery aging depends on many factor, namely the maximum charging voltage, and the discharge current level and rate [41,45]. Discharging the cell at higher currents and to deeper depths of

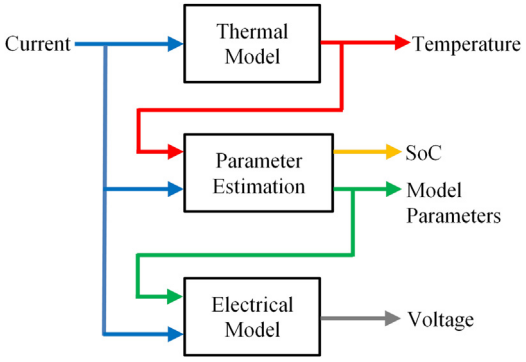

Fig. 7. Block diagram of control-oriented Li-ion battery model.

discharge (DoD) also results in shorter cell life. A descriptive measure of the discharge current level and rate is the average and the standard deviation of state of charge (SoC), respectively [46]. In addition, the battery temperature has an influence on its aging. The increase in temperature results in faster consumption of the battery reactants causing them to be consumed quickly, and hence shortening the cell life [47].

The battery aging model must account for all the aging factors discussed above in order to ensure accuracy. In this paper, the battery aging model presented in Ref. [46] was used. This model has been validated in Ref. [48] against real test data for the specific battery cell A123 ANR26650M1A herein Ref. [10].

The battery aging model represents the damage to its life by variable (L), which can vary from 0 (new) to 1 (dead). Normally, $L = 0.2$ is used as a measure for end of useful life, resulting in 80% of the nominal capacity [10,11]. L is calculated using the aging model in three stages: the first one (L_1) accounts for swing in SoC, the second one (L_2) accounts for average SoC, and the third stage (L_3) accounts for temperature effects. They are given by Ref. [46]:

$$L_1 = K_{co} \cdot N \cdot e^{(SoC_{dev}-1)T_{ref}/K_{ex}/T_B} \quad (5)$$

$$L_2 = L_1 \cdot e^{K_{SoC}(SoC_{avg}-0.5)} \cdot (1 - L_i) \quad (6)$$

$$L_3 = L_2 \cdot e^{K_T(T_B - T_{ref})} \cdot \frac{T_{ref}}{T_B} \quad (7)$$

The accumulative change in life aging parameter after M time intervals is given in Ref. [46]:

$$L(M) = \sum_{m=1}^{M} L_3(m) \quad (8)$$

All the empirical constants K_{co}, K_{ex}, K_{SoC}, and K_T are battery specific, and must be obtained from test data. A battery life test was performed in Ref. [48]. The values of battery aging model constants are tabulated in Table 3. The State of Health (SoH) of a battery is related to aging by Ref. [49]:

$$SoH = 1 - \frac{L}{0.2} \quad (9)$$

which decreases over time. SoH is equal to 1 at the beginning of life (BoL) and equal to 0 at end of life (EoL), *i.e.* $L = 0.2$.

With the help of the above-validated models, a detailed simulation has been carried out for battery life estimation of the fuel cell-battery hybrid DERs in microgrid.

4. Problem identification

Upon microgrid system simulation, it was observed that the dynamic responses of the four fuel cell-battery hybrid DERs to the crusher–conveyor load are varied. Individual units' responses are highly influenced by their relative 'electrical' locational placements within the microgrid. This is due to the differing underlying interface reactances between the DERs and the crusher–conveyor load [14]. Ideally, it is desired for each DER's power profile to follow the change in the load abruptly without any delays, as shown in Fig. 8(a). This case is hypothetical since the current cannot change instantaneously across the reactances embedded in the system (*cf.* Fig. 2). This case will be considered as an "ideal" case throughout the text and the battery aging results for this case indicate that all the batteries age at the exact same rate and that they all reach EoL after 21664 cycles, as illustrated in Fig. 8(b).

The above ideal case is not a realistic scenario in an interconnected power system. Therefore, a time-domain simulation was carried out in MATLAB®/Simulink™ with the power network simulated in SimPowerSystems™ toolbox for a worst case scenario, taking into account the various network reactances in the microgrid (*cf.* Fig. 2). For this case, labeled as *baseline*, the smallest DER was considered to be closer to the crusher–conveyor. Fig. 9 shows the dynamic response of the microgrid supplying the crusher–conveyor load. The battery aging results for this realistic case indicates that each DER's battery reaches its EoL at a distinct time. The reasons are discussed in further detail below.

As shown in Fig. 9, the difference in the transient responses resulted in significant variations in the utilization of the Li-ion batteries in different DERs. The more 'electrically' closer a DER unit is to the load, the more stress is placed on its battery. This causes differences in SoC curves of the various batteries, as shown in Fig. 10(a). It is due to a higher discharge current, which implies a higher rate of energy conversion leading to heat losses [50]. This eventually results in a rise in the battery temperature as shown in Fig. 10(b), where the temperature of Battery 1 shot up to a peak value of 60 °C from an ambient temperature of 35 °C.

Table 3
Battery aging model constants.

Constant	Name	Value
K_{co}	Coefficient of throughput	3.66×10^{-5}
K_{ex}	Exponent of DoD	0.717
K_{SoC}	Coefficient of SoC_{avg}	0.916
K_T	Thermal coefficient	0.0693
T_{ref}	Ref battery temperature	35 °C

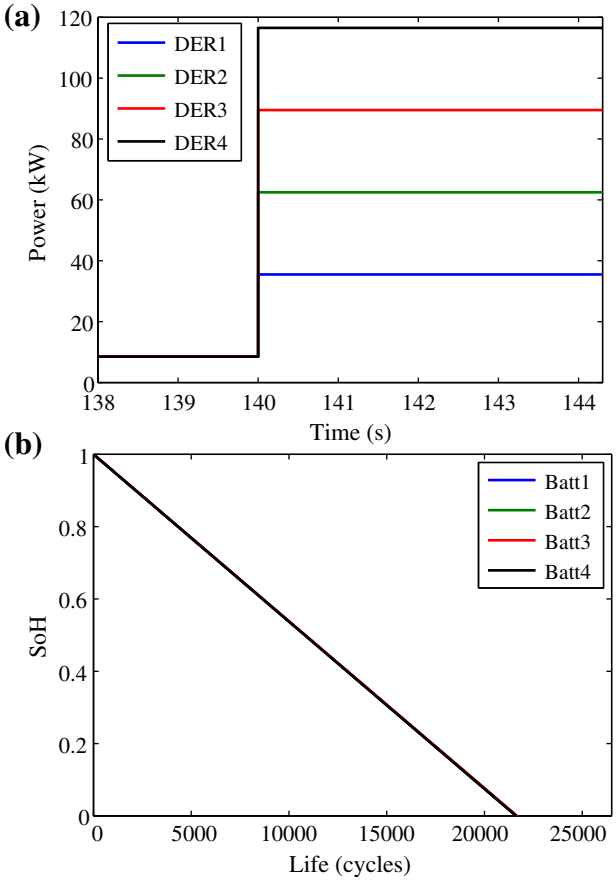

Fig. 8. Ideal case (a) power profile, and (b) battery state of health (SoH).

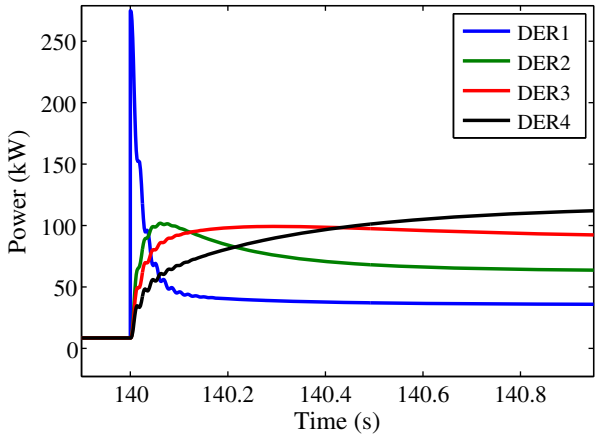

Fig. 9. Power response characteristic.

According to the battery aging model, SoC and temperature are the two main factors affecting the rate of aging of the battery. By applying the SoC and temperature data obtained earlier from time-domain simulation of microgrid to an offline battery aging model also developed in MATLAB®, the resulting aging factor for the four DER batteries was obtained as shown in Fig. 10(c). This figure illustrates a definite unbalance in the accumulation of the aging factor. By calculating the accumulated age over the time, the aging results depicted in Fig. 10(d) show that significant variations in battery age occur for the four DERs. Assuming that each battery replacement is carried out after its EoL, it has been observed that Battery 1 reached EoL after 11,627 cycles, which is almost one half the hypothetical estimated lifetime in the "ideal" case. Further, Battery 2, Battery 3, and Battery 4 survived until 16,928 cycles, 19,791 cycles, and 25,106 cycles, respectively. However, it is to be noted that if Battery 1 does not get replaced after its EoL of 11,627 cycles, the supply network to the crusher–conveyor can actually collapse within a shorter period than estimated above. This is because the remaining three surviving batteries may not be able to themselves meet the challenging load requirement, thereby leading to a series of cascading failures and eventually resulting in the shutdown of the entire industrial power system.

5. Strategies for balancing the battery cycle life in microgrid

In this section, a balancing strategy to the battery life discrepancy problem is proposed by employing the *Flexible Distribution of EneRgy and Storage Resources* (FDERS) framework. More explanation on the concept of FDERS along with quantitative and qualitative analysis was presented in Refs. [14,51]. A detailed step-by-step procedure to realize the synthesized virtual reactances and the reconfiguration technique in FDERS was discussed in Ref. [52].

FDERS transforms a *fixed* electrical power network into a *flexible* one for achieving potential savings in terms of increased DER lifetime, optimal energy storage deployment, enhanced controllability and improved system robustness [14]. This flexibility is achieved by controlling the 'electrical' locational placements of DERs within the microgrid. It is realized, as shown in Fig. 11, by means of *synthesized 'virtual' reactances* $X_{k\text{-add}}$, which can be accomplished in the DER controller by modifying its voltage reference from $\overrightarrow{v}^{*}(t)$ to $\overrightarrow{v}^{'*}(t)$. As a result, the net reactance between the kth DER and load will be $X_k = X_{k0} + X_{k\text{-add}}$ – that can be smoothly adjusted. In this way, the *pecking order* of DER positions as seen from the load can be effortlessly changed. Although the concept of virtual reactance has been applied earlier by several authors for other purposes, it has been

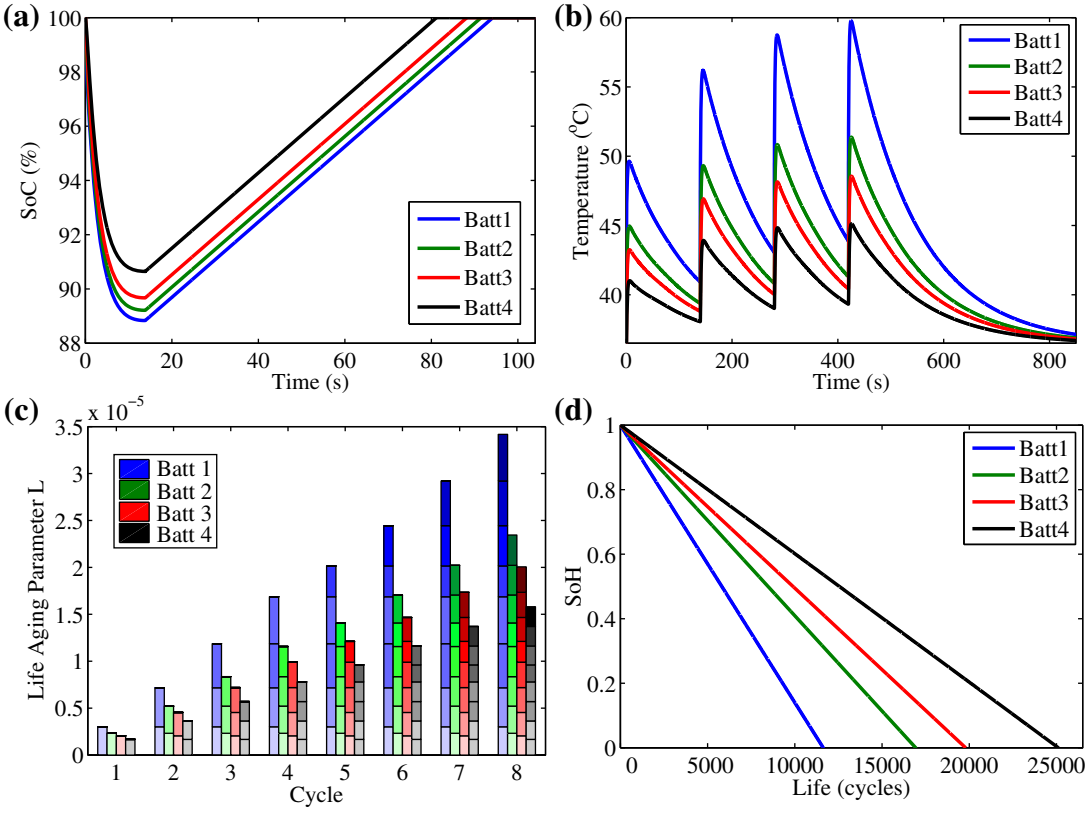

Fig. 10. Baseline case (a) battery SoC, (b) battery temperature, (c) life aging parameter for batteries, and (d) battery SoH.

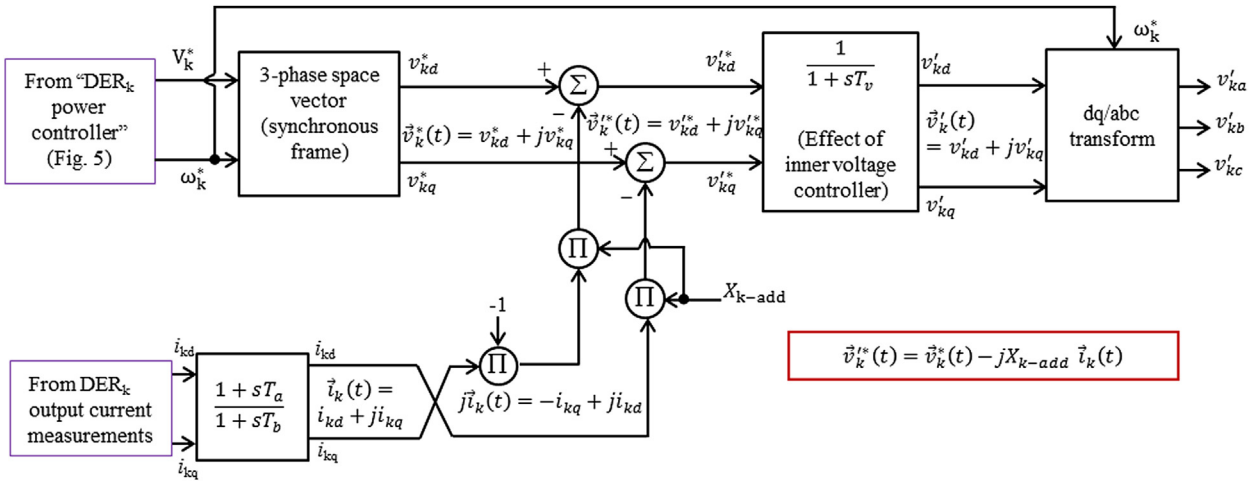

Fig. 11. Synthesis of variable reactance in the DER's controller.

employed in the FDERS with a different intent - to facilitate a change of the pecking order or hierarchy among the interconnected DERS.

The control of PWM inverter-based DER units is done by means of a multi-loop regulator which outer loop is as shown in Fig. 5, and the inner loop consists of voltage regulator for the inverter output. The bandwidth of inner loop voltage regulator is limited by the inverter switching frequency, and that of outer power control loop is one order further lower. It was observed, as experimental tests showed in Refs. [25], that an inverter operating at 4-kHz switching frequency had limited the bandwidth of inner loop voltage regulator to around 200 rad s^{-1}. Accordingly, the transfer function between commanded voltage (V_k^*) and actual voltage (V_k) in Fig. 11 can be approximated as a first-order lag function with time constant $T_v = (200)\ s^{-1} = 5$ ms. Also a lead-lag transfer function was included to compensate for any delays in the current measurement.

This paper presents three approaches to accomplish the balancing of battery aging to varying degrees in the microgrid as follows.

5.1. Periodic cycling – Approach A

In this approach, all the DERs are cycled periodically to change their 'electrical' positions according to the four orders shown in Table 4, which contains the various positions considered for the four DERs in the context of the microgrid in Fig. 2. In the first order, *i.e.* "Order I," no virtual reactances are added to the system; therefore, the response is unchanged from the baseline response (*cf.* Fig. 9). In "Order II", it is DER2's turn to take the lead and DER1's turn to draft in the last position. Likewise, the sequence continues for "Order III" and "Order IV" where DER3 and DER4 take turns to lead, respectively. The values of virtual reactances ($X_{k\text{-add}}$) necessary to achieve these four cycles are tabulated in Table 4, and the sequence repeats itself never ending. The cycling frequency in this approach was set to once per cycle, meaning that all these four orders will take place in 4 consecutive cycles, refer to Table 1.

Table 4
Settings of parameters for cycling.

Order	Reactance, X (Ω)	DER1	DER2	DER3	DER4
I	Physical (X_{k0})	0	0.18	0.27	0.46
	Virtual ($X_{k\text{-add}}$)	0	0	0	0
	Total ($X_k = X_{k0} + X_{k\text{-add}}$)	0	0.18	0.27	0.46
	Position	**1**	**2**	**3**	**4**
II	Physical (X_{k0})	0	0.18	0.27	0.46
	Virtual ($X_{k\text{-add}}$)	0.46	−0.18	−0.09	−0.19
	Total ($X_k = X_{k0} + X_{k\text{-add}}$)	0.46	0	0.18	0.27
	Position	**4**	**1**	**2**	**3**
III	Physical (X_{k0})	0	0.18	0.27	0.46
	Virtual ($X_{k\text{-add}}$)	0.27	0.28	−0.27	−0.28
	Total ($X_k = X_{k0} + X_{k\text{-add}}$)	0.27	0.46	0	0.18
	Position	**3**	**4**	**1**	**2**
IV	Physical (X_{k0})	0	0.18	0.27	0.46
	Virtual ($X_{k\text{-add}}$)	0.18	0.09	0.19	−0.46
	Total ($X_k = X_{k0} + X_{k\text{-add}}$)	0.18	0.27	0.46	0
	Position	**2**	**3**	**4**	**1**

A sample of the batteries SoC under this approach with "Order II" is shown in Fig. 12(a). A sample of temperature profiles of four consecutive cycles is also shown in Fig. 12(b). After a detailed battery aging analysis as described in the previous section, the life aging parameters and the estimated batteries lifetimes under Approach A were obtained as shown in Fig. 12(c) and (d), respectively. The life of Battery 1 was extended to 17,237 cycles from 11,627 cycles of baseline. However, this was at the cost of the life of Battery 4, which suffered from a loss of about 3000 cycles as compared to its baseline lifetime.

5.2. Power rating-weighted cycling – Approach B

Another approach that provided an improved battery cycle life performance was when the ratio of number of cycles for each *Order* is made proportional to the ratio of the DER unit's rated power. Accordingly, the cycles are determined as (number of cycles for "Order I"):(∼ "Order II"):(∼"Order III"):(∼"Order IV") = 30 kW:60 k :90 kW:120 kW which can be further simplified as equal to 1:2:3:4. In other words, "Order I" occurs for one cycle, then "Order II" takes place for the next two cycles, and likewise the sequence goes on for "Order III" and "Order IV", respectively. (Note: the *Orders* have been described earlier in Table 4).

The simulation results under Approach B show that the batteries demonstrated relatively more balanced SoC and therefore temperature. A sample of both SoC and temperature is shown in Fig. 13(a) and (b), respectively. As a result, the aging rates were also more evenly distributed, as shown in Fig. 13(c). Since this pattern repeats itself for the system operation, the aging rates are expected to be maintained constant over time. The battery state of health (SoH) curves for this approach is shown in Fig. 13(d). It is evident from these results that Approach B provides improved balancing of battery lifetimes as compared to Approach A. In

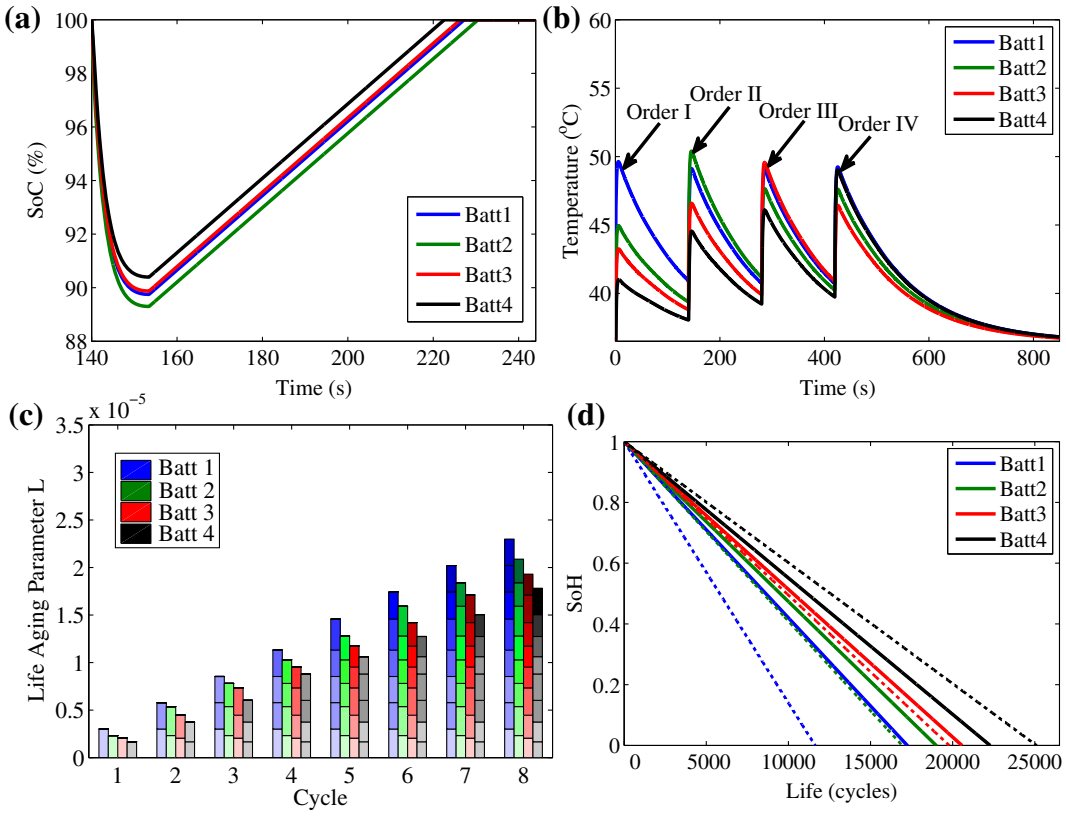

Fig. 12. Approach A (a) battery SoC, (b) battery temperature, (c) life aging parameter for batteries, and (d) battery SoH compared with baseline (dotted lines).

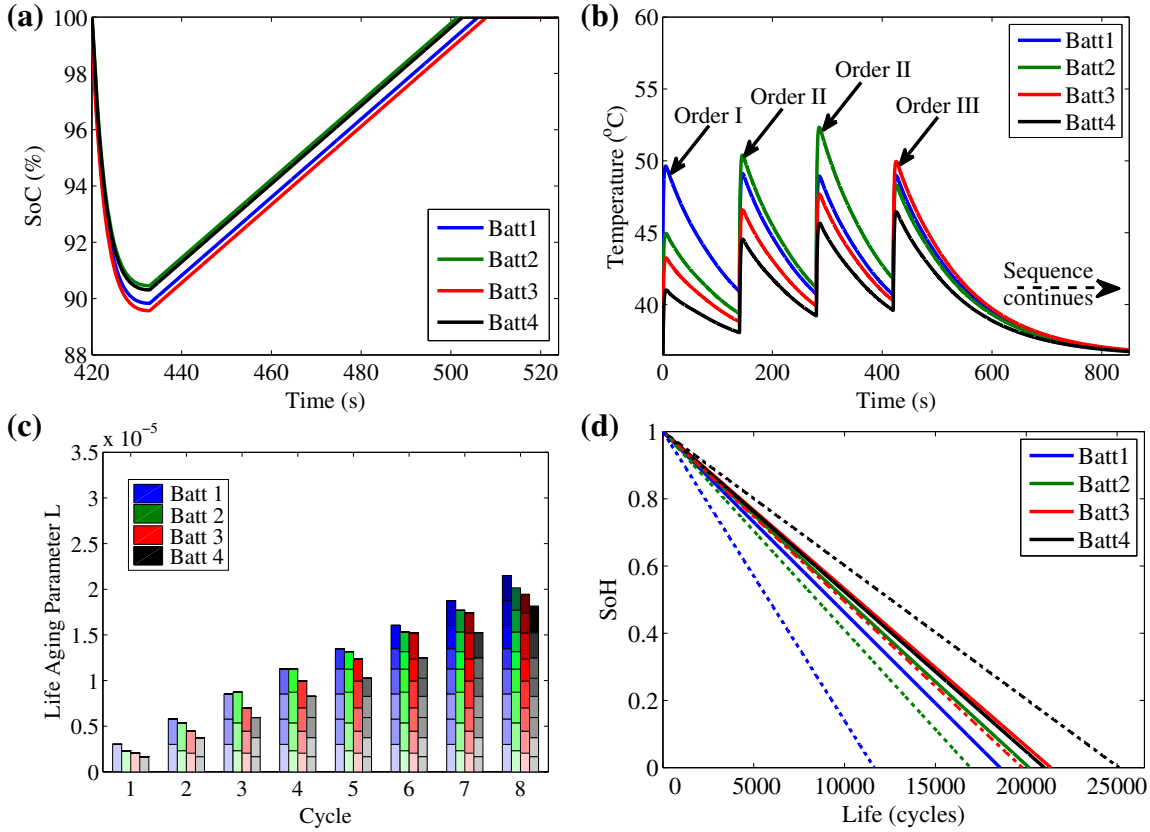

Fig. 13. Approach B (a) battery SoC, (b) battery temperature, (c) life aging parameter for batteries, and (d) battery SoH compared with baseline (dotted lines).

Table 5
Settings of parameters for cycling – Approach C.

Order	Reactance, X (Ω)	DER1	DER2	DER3	DER4
III	Physical (X_{k0})	0	0.18	0.27	0.46
	Virtual ($X_{k\text{-add}}$)	0.27	0.28	−0.27	−0.28
	Total ($X_k = X_{k0} + X_{k\text{-add}}$)	0.27	0.46	0	0.18
	Position	**3**	**4**	**1**	**2**
V	Physical (X_{k0})	0	0.18	0.27	0.46
	Virtual ($X_{k\text{-add}}$)	0.46	0.09	−0.09	−0.46
	Total ($X_k = X_{k0} + X_{k\text{-add}}$)	0.46	0.27	0.18	0
	Position	**4**	**3**	**2**	**1**

particular, the estimated lifetime of Battery 1 is 18,561 cycles for Approach B as compared to 17,237 cycles for Approach A. Moreover, Battery 2 and Battery 3 have also gained more life under this approach. On the down side, Battery 4 sacrifices some of its lifetime to the advantage of the other three batteries – the estimated lifetime of Battery 4 dropped by 2000 cycles in this approach relative to Approach A.

5.3. Power rating-levelized cycling – Approach C

A third notable approach that gave promising results is based on isolating into two levels the higher rated DERs and the lower rated ones, to cycle within the leading two positions and lagging two positions, respectively. Accordingly, the leading/first two 'electrical' positions, *i.e.* positions 1 and 2, are operated by the higher rated DER4 and DER3, respectively. Similarly, the lagging/last two 'electrical' positions, *i.e.* positions 3 and 4 are operated by the lower rated DER2 and DER1, respectively. For the purpose of this approach, "Order III" was borrowed from Table 4 as it represents the condition in which DER3 leads DER4 in the upper level whereas DER2 leads DER1 in the lower level. The opposite of that is a newly introduced order given as "Order V". Table 5 gives the details of the parameters needed for these two orders. The cycling in the approach alternates at the rate of 2:1 to stress DER4 more than DER3 as it has larger rate power. In other words, "Order III" occurs for one cycle, then "Order V" takes place for the next two cycles; and this sequence repeats itself with a total isolation between the two levels.

This concept of levelizing based on DERs rated power paid off very well in further converging SoC resulting in more homogenous temperatures, as shown in Fig. 14(a) and (b), respectively. Therefore, the gap between the aging rates of all batteries in the microgrid became smaller, as indicated by the battery life aging parameter, shown in Fig. 14(c). By computing the accumulative age over the cycles under this approach, the overall battery SoH curves were brought closer to ideal case results as illustrated in Fig. 14(d). Particularly, the estimated lifetime of Battery 1 is 21,408 cycles as compared to 17,237 cycles and 18,561 cycles for Approach A and Approach B, respectively. The estimated lifetimes of the four batteries are brought close to each other to achieve a 76% improvement in the system's lifetime as compared to the baseline.

Thus, it has been observed that the three FDERS-based approaches have a major impact on the SoC (and ΔDoD). This is because all the batteries get stressed in a more balanced manner. All the presented approaches changed the ΔDoD of each battery according to its position (and rating) at each cycle without implementing any physical change to the system; this was done by means of lowering the average SoC, and, consequently, lowering the temperature. In all approaches, the accumulated batteries' lifetimes were balanced to varying degrees depending on the cycling sequence, pattern, and occurrence.

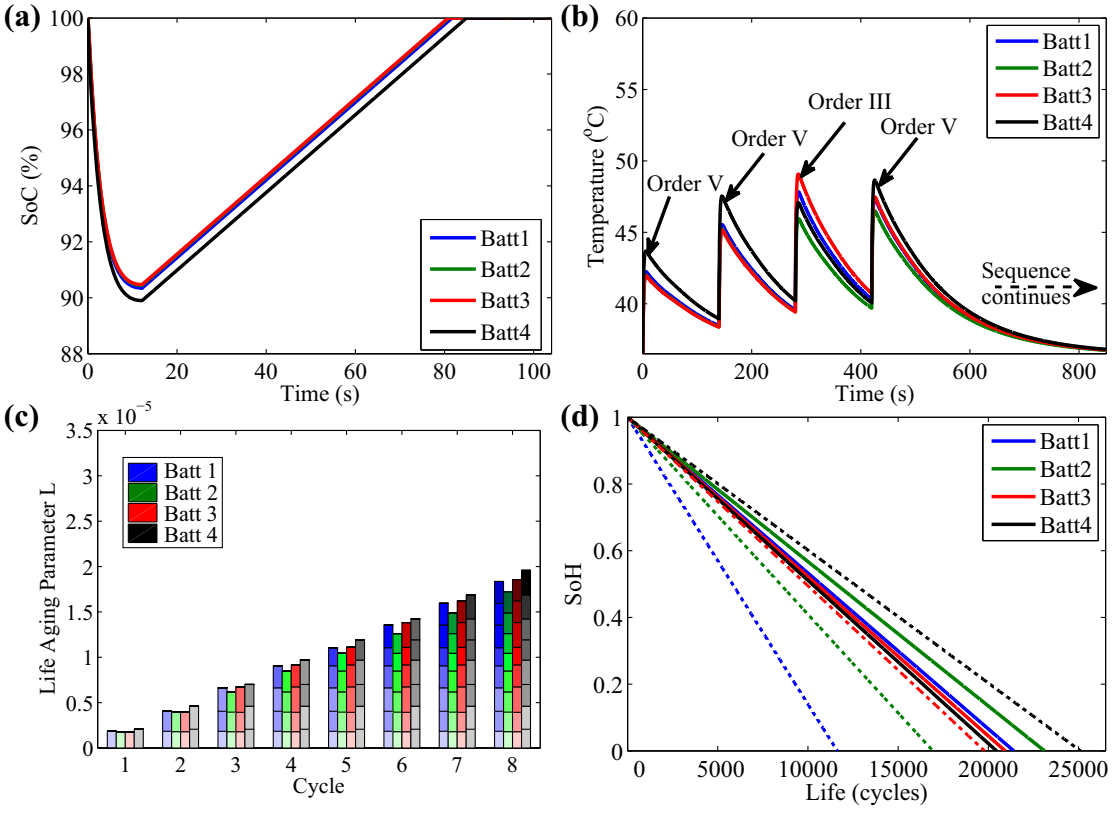

Fig. 14. Approach C (a) battery SoC, (b) battery temperature, (c) life aging parameter for batteries, and (d) battery SoH compared with baseline (dotted lines).

Table 6
Battery cycle life comparison between the three approaches (in cycles).

	Batt 1	Batt 2	Batt 3	Batt 4	Life extension
Baseline	11627	16928	19791	25106	0%
Approach A	17237	18995	20565	22278	48%
Approach B	18561	20157	21353	20997	60%
Approach C	21408	23111	20936	20453	76%
Ideal Case	21664	21664	21664	21664	86%

Approach A presented a first possible implementation of FDERS toward achieving an equalization of the battery age rates. While Approach A may work for the case of four identical DERs, its ability to balance a broad ranging and realistic scenario of multiple DERs would not be sufficient. Changing the 'electrical' positions based on DER power ratings, in Approach B, resulted in further convergence of batteries lifetimes toward the theoretical results. It was originally believed that Approach B would immaculately work in the case of multiple DERs of dissimilar ratings. However, Approach C offered the best solution to the discrepancy in batteries lifetime problem through levelizing the DERs according to their ratings. This approach resulted in better equalizing the batteries lifetimes in values close to the ideal case. Also, the concept introduced in Approach C can be easily scaled to a larger microgrid with multiple DERs by assuming more levels and assigning the DER units to these levels according to their power ratings.

The results of all the above FDERS-based battery life balancing strategies analyzed in this section are summarized in Table 6. For the purpose of comparison, the baseline and ideal cases have also been included. As observed in this table, Approach C provides the best and practicable case with 76% improvement in the system's lifetime as compared to the baseline. This performance by Approach C is a realistic scenario that is close to the ideal case of 86% improvement in the system's life.

In all the analysis carried out so far, a key assumption has been made that each battery is replaced immediately after its EoL is reached. It is to be noted that if the replacement of Battery 1 (for example) is not made at the designated time, the supply network to the crusher–conveyor can actually collapse within a shorter period than was estimated. This is because the remaining three surviving batteries may not be able to themselves meet the challenging load requirement, thereby leading to a series of cascading failures and eventually resulting in the shutdown of the entire industrial power system. Moreover, the nearly equalized battery cycle life of all four DER units makes it easy for field service engineers to make all battery replacements at the same time.

6. Conclusions

Distributed Energy Resources (DERs) and microgrids are being increasingly favored to cover the growing needs of high energy consumers in the modern power grid. Small-rated rotating machine based DERs as well as electrochemical DERs such as fuel cells have long start-up time and poor transient response due to their intrinsic characteristics. Therefore, such DERs are generally supplemented with energy storage systems. This paper analyzed the battery cycle life in a microgrid consisting of four distantly located small-rated fuel cell-battery hybrid DERs for supplying a large and fluctuating crusher–conveyor load when power from the main (grid) utility was not present. The simulation of MATLAB®/Simulink™ model of the system, during the baseline operation in the traditional fixed network, showed significant variations in the utilization of the Li-ion batteries due to the difference in the transient responses and dynamics of the microgrid. These differences caused unbalance in batteries' SoC and temperatures which led to a clear unbalance in their estimated lifetime. As a solution, this paper demonstrated various strategies to balance the battery cycle life by creating a cooperative framework known as Flexible Distribution of EneRgy and Storage Resources (FDERS). Such a framework offers flexibility that is incorporated by means of synthesized 'virtual' reactances and controllable frequency/active power droop gains within the DER controllers. The strategy followed was to change the virtual reactance in order to rotate the 'electrical' position of all fuel cell-battery hybrid DERs with respect to the load. Three approaches were presented for balancing the batteries lifetimes – all of these were based on changing the ΔDoD of each battery according to its position and rated power at each cycle through *in-situ* reconfiguration. In the three approaches, the accumulated batteries ages were balanced by varying degrees depending on the cycling sequence, pattern, and occurrence. The results after applying these solutions showed that the lifetime of the most susceptible battery can be extended by 76% of baseline, which is very close to the ideal case of 86% of baseline.

References

[1] H. Jiayi, J. Chuanwen, X. Rong, Renew. Sustain. Energy Rev. 12 (2008) 2472–2483.
[2] R.H. Lasseter, in: PESC, 2004, pp. 4285–4290.
[3] R.H. Lasseter, IEEE Power Eng. Soc. (2002) 305–308.
[4] E. Achenbach, J. Power Sources 57 (1995) 105–109.
[5] L. Gao, Z. Jiang, R.A. Dougal, J. Power Sources 130 (2004) 202–207.
[6] A. Jossen, J. Garche, H. Doering, M. Goetz, W. Knaupp, L. Joerissen, J. Power Sources 144 (2005) 395–401.
[7] B. Saha, K. Goebel, in: PHM Conference, 2009.
[8] R. Spotnitz, J. Power Sources 113 (2003) 72–80.
[9] G.L. Plett, L. Gregory, J. Power Sources 134 (2004) 277–292.
[10] H.J. Bergveld, W.S. Krujit, P.H.L. Notten, Battery Management Systems: Design by Modelling, Springer, 2002.
[11] M. Dubarry, V. Svoboda, R. Hwu, B.Y. Liaw, J. Power Sources 165 (2007) 566–572.
[12] A.M. Bernardes, D.C.R. Espinosa, J.A.S. Tenório, J. Power Sources 130 (2004) 291–298.
[13] M. Contestabile, S. Panero, B. Scrosati, J. Power Sources 92 (2001) 65–69.
[14] M.S. Illindala, H.J. Khasawneh, A. Renjit, IEEE Ind. Appl. Mag. (2014) (in press).
[15] P.B.S. Lissaman, C.A. Schollenberger, Science 168 (1970) 1003–1005.
[16] H. Weimerskirch, J. Martin, Y. Clerquin, P. Alexandre, S. Jiraskova, Nature 413 (2001) 697–698.
[17] C.R. Kyle, Ergonomics 22 (1979) 387–397.
[18] A.G. Edwards, W.C. Byrnes, Med. Sci. Sports Exerc. 39 (2007) 170–176.
[19] J. Brisswalter, C. Hausswirth, Int. J. Sports Physiol. Perform. 3 (2008) 3–15.
[20] R.E. Henry, in: IEEE I & CPS, 2003, pp. 18–32.
[21] C.T. Hsu, IEEE Trans. Ind. Appl. 39 (2003) 1436–1441.
[22] C.T. Hsu, IEEE Trans. Ind. Appl. 47 (2011) 1527–1535.
[23] R.E. Henry, in: IAS Conference, 2004, pp. 750–757.
[24] Data sheet MD1000001-02 for ANR26650M1, A123 systems. www.a123systems.com.
[25] M.S. Illindala, in: University of Wisconsin-Madison, 2005.
[26] A. Renjit, M. Illindala, R. Lasseter, M. Erickson, D. Klapp, in: IEEE ECCE, 2013, pp. 1640–1646.
[27] S.J. Ahn, J.W. Park, I.Y. Chung, S.I. Moon, S.H. Kang, S.R. Nam, IEEE Trans. Power Delivery 25 (2010) 2007–2016.
[28] J.K. Steinke, IEEE Trans. Energy Convers. 14 (1999) 649–654.
[29] Y.P. Chang, C.J. Wu, IEEE Power Eng. Soc. (2003) 68–72.
[30] Z. Jiang, L. Gao, M.J. Blackwelder, R.A. Dougal, J. Power Sources 130 (2004) 163–171.
[31] Z. Jiang, L. Gao, R.A. Dougal, IEEE Trans. Energy Convers. 22 (2007) 507–515.
[32] A.J. Wood, B.F. Wollenberg, Power Generation Operation and Control, second ed, John Wiley & Sons, 1996.
[33] K. Subramanyan, U.M. Diwekar, J. Power Sources 142 (2005) 103–116.
[34] H. Misawa, Y. Hirotake, in: U.S., 1992.
[35] J. Padulles, G.W. Ault, J.R. McDonald, J. Power Sources 86 (2000) 495–500.
[36] Y. Zhu, K. Tomsovic, Electr. Power Syst. Res. 62 (2002) 1–11.
[37] H.J. Khasawneh, in: Mechanical Engineering Department, The Ohio State University, 2011.
[38] Y. Hu, S. Yurkovich, Y. Guezennec, B.J. Yurkovich, J. Power Sources 196 (2011) 449–457.
[39] G.L. Plett, IEEE Trans. Veh. Technol. 53 (2004) 1586–1593.
[40] F.P. Incropera, D.P.D. Witt, T.L. Bergman, A.S. Lavine, Fundamentals of Heat and Mass Transfer, sixth ed., John Wiley & Sons, 2006.

[41] D. Linden, T.B. Reddy, Handbook of Batteries, third ed., McGraw-Hill Professional, 2001.
[42] M. Broussely, S. Herreyre, P. Biensan, P. Kasztejna, K. Nechev, R.J. Staniewicz, J. Power Sources 97 (2001) 13–21.
[43] M. Broussely, P. Biensan, F. Bonhomme, P. Blanchard, S. Herreyre, K. Nechev, J. Power Sources 146 (2005) 90–99.
[44] J. Vetter, P. Novák, M.R. Wagner, C. Veit, K.C. Mölle, J.O. Besenhard, M. Winter, M. Wohlfahrt-Mehrens, A.H.C. Vogler, J. Power Sources 147 (2005) 269–281.
[45] G. Ning, R.E. White, B.N. Popov, Electrochim. Acta. 51 (2006) 2012–2022.
[46] A. Millner, in: IEEE CITRES, 2010, pp. 349–356.
[47] S. Santhanagopalan, Q. Zhang, K. Kumaresan, R.E. White, J. Electrochem. Soc. 155 (2008) A345–A353.
[48] S. Peterson, J. Apt, J. Whitacre, J. Power Sources 195 (2010) 2385–2392.
[49] C. Guenther, B. Schott, W. Hennings, P. Waldowski, M.A. Danzer, J. Power Sources 239 (2013) 604–610.
[50] D. Bernardi, E. Pawlikowski, J. Newman, J. Electrochem. Soc. 132 (1985) 53–63.
[51] H.J. Khasawneh, M.S. Illindala, in: IEEE ECCE, 2013, pp. 43–50.
[52] A. Renjit, M.S. Illindala, in: IEEE ECCE, 2013, pp. 2378–2384.